Hindawi
Modelling and Simulation in Engineering
Volume 2022, Article ID 2105847, 13 pages
https://doi.org/10.1155/2022/2105847

Research Article

Low-Frequency Analytical Model of Superconducting Magnet Impedance

Michele Martino

Accelerator Systems (SY) Department, CERN, Geneva, Switzerland

Correspondence should be addressed to Michele Martino; michele.martino@cern.ch

Received 27 June 2022; Accepted 23 September 2022; Published 7 November 2022

Academic Editor: Heng Bo Jiang

A superconducting magnet for particle accelerators is often modeled as an ideal inductor, as it indeed exhibits a completely negligible resistance; this is fully satisfactory, as an example, for control purposes, as the time constant formed by the magnet inductance and the resistance of normal conducting cables connecting it to the power converter accurately describe the essentially dominant dynamics of the circuit. Such a model would however fail to correctly represent the noise attenuation mechanism at play in practical superconducting magnets, which also include a vacuum pipe or a beam screen in the inner part of the aperture, an iron yoke on the outer part, and, potentially, a stainless steel or aluminum collar in between. Even at relatively low frequencies, a more accurate model is therefore needed. A sufficiently general one is proposed and illustrated.

1. Introduction

This work is aimed at improving the impedance modeling of superconducting magnets for particle accelerators in the low-frequency range (i.e., from DC to a few kHz). Its scope is also limited to individual magnet modelling; in practical magnet circuits, several magnets might be connected in series so the circuit can have significant physical length; its impedance might then need to be modelled as a transmission line which outgoes the scope of this work.

Availability of a low-frequency model is relevant as it allows for the proper specification of noise performances, within the above-mentioned range of frequencies, in magnet circuits of particle accelerators, as an example for the HL-LHC (High-Luminosity Large Hadron Collider) project [1–3]. Clearly, noise in higher frequency can also have a significant impact on the beam, but such an analysis far outgoes the scope of this contribution and would need to be carried out *decade by decade* [3] as different phenomena come to play in different frequency ranges and from different causes (not necessarily related to the noise produced by the power converters). The exact type of noise analysis carried out in this work will be clarified in the following; its focus is, however, limited to the impact of voltage noise (inevitably produced by power converters) on the magnetic field to be experienced by the beam. The proposed model should nevertheless be considered instrumental to further analysis on beam dynamics figures of merit which however outgoes the scope of this work. It is fundamentally a generalization of the content presented in the seminal paper [4] carried out with a more rigorous and coherent notation. Indeed, in [4], the frequency domain, Laplace domain, and time domain notations are often used all at once, which does not allow for a concise and rigorous analytical formulation of the overall magnet impedance as seen by the circuit terminals (i.e., by the power converter terminals). Such a drawback is overcome here, and several generalizations are also presented and discussed together with an illustrative case study.

The content is organized as follows: in Section 2, the basic assumptions are presented together with the relevant results and their complete derivation. In Section 3 the presented results are translated into a simple equivalent circuit, generalizing the one presented in [4]. Particular emphasis is given to the noise analysis which can be thought of as the main goal of this work. A dominant effect is identified and described in detail in Section 4.At the same time, an exact formulation is presented for an ideal dipole magnet, and a

simple case study, from the Large Hadron Collider, is discussed to better illustrate the soundness of the approximations introduced. With regard to important practical features, only nominal operating conditions are considered, as they are the only relevant ones for the quality of circulating beams. The impact of the different structural elements (collars, yoke, etc.) on quench events or on faults (electromechanical, thermal, etc.), although quite critical for practical operation, is therefore not investigated herein. The presence of an iron yoke and the impact of magnetoresistance, together with a more accurate calculation of the inductance (to the best of the author's knowledge, such a formula has not been presented elsewhere), are briefly addressed in the Appendix to help readability. Summarizing remarks are finally given in Section 5.

2. Low-Frequency Field Modeling

2.1. Quasistationary Magnetic Modelling. The fundamental assumption herein is that the displacement current density $\mathbf{J}_{\mathrm{D}} = \partial \mathbf{D}/\partial t$ is negligible with respect to the intensity of the magnetic field internal stray capacitive effects (in the nF range), such as, for example, the ones between coils and stainless steel or aluminum collars, are herein neglected as they normally kick in at higher frequencies (tens of kHz) ($\mathbf{D}$ being the electric displacement field). Furthermore, the physical dimensions of superconducting magnets are such that no propagation phenomena need to be considered. Maximum physical dimensions considered are indeed negligibly small compared to the shortest reasonable wavelength; as an example, one can consider a maximum frequency of 1 MHz (well beyond the range of frequencies of interest in this work) for which the corresponding wavelength would be of about 300 m, so a 10 m-long magnet would still be accurately approximated.

With both these conditions, the modeling presented here falls within the so-called *Quasistationary Magnetics*.

2.2. 2D Modelling. In addition to the above hypotheses, to further simplify the modeling, the lengths of magnets (along the conventional axis z) are considered large enough, so a 2D approximation is deemed satisfactory (edge effects are neglected).

2.3. Absence of Nonlinear Materials. All materials considered here are assumed to be linear. The more realistic case of superconducting magnets with a concentric iron yoke is discussed in the Appendix although a full investigation of its nonlinear and frequency-dependent impact on the presented results is beyond the scope of this work. Furthermore, conductive materials experience magnetoresistance; this is also briefly addressed in the Appendix; although the impact of this effect is likely to be smaller than the one caused by the saturation of the iron yoke, its full investigation is beyond the scope of the work presented.

2.4. Thin Layer Approximation. Following closely the analysis conducted in [4], and using the same notation, it can be shown that a current $I(s)$ (with s being the variable of the Laplace domain, the initial conditions are all assumed to be zero) flowing perpendicularly through an annulus having an average radius $r = b$ and a thickness Δ_b, as shown in Figure 1, produces, for a magnet of order n ($n = 1$ for a dipole, $n = 2$ for a quadrupole, etc.), a magnetic vector potential:

$$\begin{aligned} A_z(r,\theta,s) &= \left(\frac{r}{b}\right)^{n\ \mathrm{sgn}\,(b-r)} A_z(b,\theta,s), \\ A_z(b,\theta,s) &= \mu_0 \frac{b\Delta_b}{2n} J_z(b,\theta,s). \end{aligned} \tag{1}$$

The quasistatic current density is

$$J_z(r,\theta,s) = \frac{N_t \cos(n\theta)}{2} I(s) \frac{1}{b\Delta_b} \delta\left(\frac{r-b}{\Delta_b}\right), \tag{2}$$

where N_t is the number of turns, and therefore, $I(s)(N_t/2)\cos(n\theta)$ represents the azimuthal current density distribution within the annulus (it is assumed that $J_z(b,\theta,s) = [N_t \cos(n\theta)/2]I(s)(1/b\Delta_b)$ as equation (2) is to be correctly interpreted as a generalized function).

It must be noted that in equation (1), the factor $b\Delta_b$ (proportional to the area of the annulus) is present both at the numerator and at the denominator; therefore, the intensity of the potential vector depends only on the intensity of the current I and its azimuthal distribution. This expedient allows factoring the expression of the potential vector, which turns out to be useful in the following; furthermore, this formulation does not have the drawback of the one proposed in [4] where the current density was expressed in Am^{-1} instead of the correct Am^{-2}.

It is probably worth highlighting the notation introduced in equation (1), and adopted throughout the work, which exploits the signum function sgn as an exponent. This is done to make the expression of the magnetic vector potential more compact, although less conventional than in [4–6], by avoiding the explicit description of two cases at each occurrence.

It is fundamental to note that the complete mathematical derivation has nevertheless been carried out assuming that the thicknesses Δ_a, Δ_b, and Δ_c are (negligibly) small compared to the respective radii a, b, and c such that all fields in the annular sections can be considered radially uniform. This clearly represents an idealization which might not always accurately represent practical superconducting magnets for particle accelerators; these aspects will be addressed, when relevant, in the next sections and in the Appendix.

2.5. Inner Conductive Layer (Beam Screen). At $r = a$ ($a < b$), there is a thin sheet of conductor with thickness Δ_a representing a so-called *beam screen* (which could also represent a simple vacuum pipe where an actual beam screen is absent). A current is induced which can be written as

$$J_z(a,\theta,s) = \sigma^i E_z = -s\sigma^i \left[A_z(a,\theta,s) + A_z^i(a,\theta,s)\right], \tag{3}$$

where σ^i is the conductivity of the layer and $A_z + A_z^i$ represents the total vector potential A_z^{tot}.

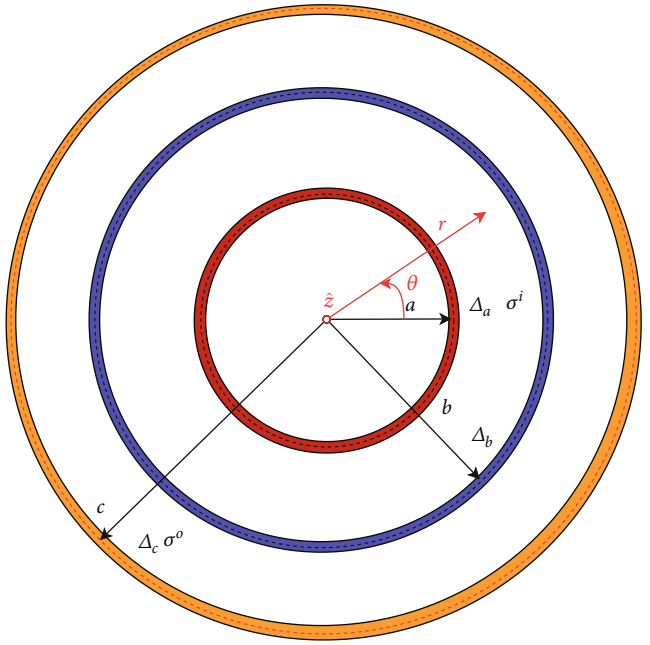

FIGURE 1: Simplified cross-section (not to scale) of an ideal superconducting magnet with superimposed adopted cylindrical coordinates): coils are located at $r = b$, an inner conductive shell (beam screen or vacuum pipe for example) is located at $r = a$, and an outer conductive shell (stainless steel or Al collar as an example) is located at $r = c$.

The dependence on θ and s will be omitted in the following. $A_z^i(r)$ can be expressed by considering the *new* source $J_z^i(a)$ as

$$\begin{aligned} A_z^i(r) &= \mu_0 \frac{a\Delta_a}{2n}\left(\frac{r}{a}\right)^{n\ \mathrm{sgn}\,(a-r)} J_z^i(a) \\ &= \mu_0 \frac{a\Delta_a}{2n}\left(\frac{r}{a}\right)^{n\ \mathrm{sgn}\,(a-r)} \left[-s\sigma^i A_z^{tot}(a)\right] \\ &= -s\sigma^i \mu_0 \frac{a\Delta_a}{2n}\left(\frac{r}{a}\right)^{n\ \mathrm{sgn}\,(a-r)} \left[A_z(a) + A_z^i(a)\right] \\ &= -s\tau_i \left[\left(\frac{r}{a}\right)^{n\ \mathrm{sgn}\,(a-r)} \mu_0 \frac{b\Delta_b}{2n}\left(\frac{a}{b}\right)^{n\ \mathrm{sgn}\,(b-a)} J_z(b) + \left(\frac{r}{a}\right)^{n\ \mathrm{sgn}\,(a-r)} A_z^i(a)\right], \end{aligned} \tag{4}$$

where

$$\tau_i = \sigma^i \mu_0 \frac{a\Delta_a}{2n} \tag{5}$$

has the dimensions of time.

$A_z^i(r)$ can therefore be rewritten as follows:

$$\begin{aligned} A_z^i(r) &= -s\tau_i \left[\left(\frac{a}{b}\right)^n \left(\frac{r}{a}\right)^{n\ \mathrm{sgn}\,(a-r)} \left(\frac{b}{r}\right)^{n\ \mathrm{sgn}\,(b-r)} \mu_0 \frac{b\Delta_b}{2n}\left(\frac{r}{b}\right)^{n\ \mathrm{sgn}\,(b-r)} J_z(b) + A_z^i(r)\right] \\ &= -s\tau_i \left[k^i(r) A_z(r) + A_z^i(r)\right], \end{aligned} \tag{6}$$

where

$$k^i(r) = \begin{cases} 1, & r \le a, \\ \left(\dfrac{a}{r}\right)^{2n}, & a < r < b, \\ \left(\dfrac{a}{b}\right)^{2n} = k_i, & r \ge b. \end{cases} \tag{7}$$

Therefore,

$$A_z^i(r) = -\frac{s\tau_i k^i(r)}{1 + s\tau_i} A_z(r). \tag{8}$$

The total vector potential in this case is $A_z^{tot}(r) = A_z^i(r) + A_z(r)$ which can be finally calculated as

$$A_z^{tot}(r) = \frac{1 + s\tau_i\left[1 - k^i(r)\right]}{1 + s\tau_i} A_z(r). \tag{9}$$

Therefore, the inner conductive layer introduces a rational transfer function (between the *source* potential vector and the *total* one) which has a pole with time constant τ_i and a zero with time constant $\tau_i[1 - k^i(r)]$. The position of the pole is determined only by the conductivity of the annulus and its area (actually, by the product of the two) together with the order of the magnet, while the position of the zero also depends on the radial coordinate r. In particular, in the interior of the conductive layer $r \le a$, $k^i(r) = 1$, the zero disappears. This implies that within the range of frequencies considered herein, the field in the interior of the conductive layer keeps being attenuated as the frequency increases.

2.6. Outer Conductive Layer (Stainless Steel or Al Collar). At $r = c$ ($c > b$), there is a thin sheet of conductor with thickness Δ_c representing a *stainless steel or Al collar* often present in the magnet design. A current is induced, which can be written as

$$J_z(c, \theta, s) = \sigma^o E_z = -s\sigma^o \left[A_z(c, \theta, s) + A_z^o(c, \theta, s)\right], \tag{10}$$

where σ^o is the conductivity of the sheet and $A_z + A_z^o$ represents the total vector potential A_z^{tot}.

$A_z^o(r)$ can be expressed by considering the *new* source $J_z^o(c)$ as

$$\begin{aligned} A_z^o(r) &= \mu_0 \frac{c\Delta_c}{2n}\left(\frac{r}{c}\right)^{n\ \mathrm{sgn}\,(c-r)} J_z^o(c) \\ &= \mu_0 \frac{c\Delta_c}{2n}\left(\frac{r}{c}\right)^{n\ \mathrm{sgn}\,(c-r)} \left[-s\sigma^o A_z^{tot}(c)\right] \\ &= -s\sigma^o \mu_0 \frac{c\Delta_c}{2n}\left(\frac{r}{c}\right)^{n\ \mathrm{sgn}\,(c-r)} \left[A_z(c) + A_z^o(c)\right] \\ &= -s\tau_o \left[\left(\frac{r}{c}\right)^{n\ \mathrm{sgn}\,(c-r)} \mu_0 \frac{b\Delta_b}{2n}\left(\frac{c}{b}\right)^{n\ \mathrm{sgn}\,(b-c)} J_z(b) + \left(\frac{r}{c}\right)^{n\ \mathrm{sgn}\,(c-r)} A_z^o(c)\right], \end{aligned} \tag{11}$$

where

$$\tau_o = \sigma^o \mu_0 \frac{c\Delta_c}{2n}. \tag{12}$$

$A_z^o(r)$ can therefore be rewritten as follows:

$$\begin{aligned} A_z^o(r) &= -s\tau_o \left[\left(\frac{b}{c}\right)^n \left(\frac{r}{c}\right)^{n\ \mathrm{sgn}\,(c-r)} \left(\frac{b}{r}\right)^{n\ \mathrm{sgn}\,(b-r)} \mu_0 \frac{b\Delta_b}{2n} \left(\frac{r}{b}\right)^{n\ \mathrm{sgn}\,(b-r)} J_z(b) + A_z^o(r) \right] \\ &= -s\tau_o [k^o(r) A_z(r) + A_z^o(r)], \end{aligned} \tag{13}$$

where

$$k^o(r) = \begin{cases} \left(\dfrac{b}{c}\right)^{2n} = k_o, & r \le b, \\ \left(\dfrac{b}{r}\right)^{2n}, & b < r < c, \\ 1, & r \ge c. \end{cases} \tag{14}$$

Hence,

$$A_z^o(r) = -\frac{s\tau_o k^o(r)}{1 + s\tau_o} A_z(r), \tag{15}$$

from which the total vector potential can be calculated as

$$A_z^{tot}(r) = \frac{1 + s\tau_o [1 - k^o(r)]}{1 + s\tau_o} A_z(r). \tag{16}$$

The outer conductive layer also introduces a rational transfer function which has a pole with time constant τ_o and a zero with time constant $\tau_o[1 - k^o(r)]$. The position of the pole, as for the inner layer, is determined only by the conductivity of the annulus and its area (actually by the product of the two) together with the order of the magnet, while the position of the zero also depends on the radial coordinate r. In particular, in the interior of the coils $r \le b$, $k^o(r) = k_o$; hence, the zero is at constant position and its time constant is smaller than the one of the pole (zero is at higher frequency w.r.t. the pole); in this case, no further attenuation of the source field is experienced beyond the frequency of the zero.

2.7. Inner and Outer Conductive Layers. In this case, the total potential vector must account for both contributions:

$$A_z^{tot} = A_z(r) + A_z^i(r) + A_z^o(r), \tag{17}$$

which will be discussed first individually and then combined in the following subsections.

2.7.1. Inner Layer Contribution.

$$\begin{aligned} A_z^i(r) &= \mu_0 \frac{a\Delta_a}{2n} \left(\frac{r}{a}\right)^{n\ \mathrm{sgn}\,(a-r)} J_z^i(a) \\ &= \mu_0 \frac{a\Delta_a}{2n} \left(\frac{r}{a}\right)^{n\ \mathrm{sgn}\,(a-r)} \left[-s\sigma^i A_z^{tot}(a)\right] \\ &= -s\sigma^i \mu_0 \frac{a\Delta_a}{2n} \left(\frac{r}{a}\right)^{n\ \mathrm{sgn}\,(a-r)} \left[A_z(a) + A_z^i(a) + A_z^o(a)\right] \\ &= -s\tau_i \left(\frac{r}{a}\right)^{n\ \mathrm{sgn}\,(a-r)} \left[\mu_0 \frac{b\Delta_b}{2n} \left(\frac{a}{b}\right)^{n\ \mathrm{sgn}\,(b-a)} J_z(b) + A_z^i(a) + \mu_0 \frac{c\Delta_c}{2n} \left(\frac{a}{c}\right)^{n\ \mathrm{sgn}\,(c-a)} J_z^o(c)\right]. \end{aligned} \tag{18}$$

Rearranging and factoring terms, it yields

$$A_z^i(r) = -s\tau_i \left[k^i(r) A_z(r) + A_z^i(r) + k_o^i(r) A_z^o(r)\right], \tag{19}$$

where

$$\begin{aligned} k_o^i(r) &= \left(\frac{a}{b}\right)^n \left(\frac{r}{a}\right)^{n\ \mathrm{sgn}\,(a-r)} \left(\frac{c}{r}\right)^{n\ \mathrm{sgn}\,(c-r)} \\ &= \begin{cases} 1, & r \le a, \\ \left(\dfrac{a}{r}\right)^{2n}, & a < r < c, \\ \left(\dfrac{a}{c}\right)^{2n}, & r \ge c. \end{cases} \end{aligned} \tag{20}$$

2.7.2. Outer Layer Contribution.

$$\begin{aligned} A_z^o(r) &= \mu_0 \frac{c\Delta_c}{2n} \left(\frac{r}{c}\right)^{n\ \mathrm{sgn}\,(c-r)} J_z^o(c) \\ &= \mu_0 \frac{c\Delta_c}{2n} \left(\frac{r}{c}\right)^{n\ \mathrm{sgn}\,(c-r)} \left[-s\sigma^o A_z^{tot}(c)\right] \\ &= -s\tau_o \left(\frac{r}{c}\right)^{n\ \mathrm{sgn}\,(c-r)} \left[A_z(c) + A_z^i(c) + A_z^o(c)\right] \\ &= -s\tau_o \left(\frac{r}{c}\right)^{n\ \mathrm{sgn}\,(c-r)} \left[\mu_0 \frac{b\Delta_b}{2n} \left(\frac{c}{b}\right)^{n\ \mathrm{sgn}\,(b-c)} J_z(b) + \mu_0 \frac{a\Delta_a}{2n} \left(\frac{c}{a}\right)^{n\ \mathrm{sgn}\,(a-c)} J_z^i(a) + A_z^o(c)\right]. \end{aligned} \tag{21}$$

Rearranging and factoring terms, it yields

$$A_z^o(r) = -s\tau_o \left[k^o(r) A_z(r) + k_i^o(r) A_z^i(r) + A_z^o(r)\right], \tag{22}$$

where

$$k_i^o(r) = \left(\frac{a}{c}\right)^n \left(\frac{r}{c}\right)^{n\ \mathrm{sgn}\,(c-r)} \left(\frac{a}{r}\right)^{n\ \mathrm{sgn}\,(a-r)} = \begin{cases} \left(\dfrac{a}{c}\right)^{2n}, & r \le a, \\ \left(\dfrac{r}{c}\right)^{2n}, & a < r < c, \\ 1, & r \ge c. \end{cases} \tag{23}$$

2.7.3. Combining Contributions. In the following, the dependence on r will be omitted unless expressly needed.

$$\begin{aligned} A_z^i &= -s\tau_i \left[k^i A_z + A_z^i + k_o^i A_z^o\right], \\ A_z^o &= -s\tau_o \left[k^o A_z + k_i^o A_z^i + A_z^o\right], \end{aligned} \tag{24}$$

$$A_z^i = -\frac{s\tau_i}{1+s\tau_i}\left[k^i A_z + k_o^i A_z^o\right],$$
$$A_z^o = -\frac{s\tau_o}{1+s\tau_o}\left[k^o A_z + k_i^o A_z^i\right]. \tag{25}$$

Two transfer functions are defined:

$$H_i(s) = \frac{s\tau_i}{1+s\tau_i}, \tag{26}$$

$$H_o(s) = \frac{s\tau_o}{1+s\tau_o}, \tag{27}$$

so that the system can be rewritten as

$$A_z^i + H_i(s)k_o^i A_z^o = -H_i(s)k^i A_z,$$
$$H_o(s)k_i^o A_z^i + A_z^o = -H_o(s)k^o A_z. \tag{28}$$

Its solution is as follows.

$$A_z^i = -\frac{k^i - k_o^i H_o(s)k^o}{1 - H_i H_o k_i^o k_o^i} H_i(s) A_z,$$
$$A_z^o = -\frac{k^o - k^i H_i(s)k_i^o}{1 - H_i H_o k_i^o k_o^i} H_o(s) A_z, \tag{29}$$

which can be expanded as follows:

$$A_z^i = -\frac{s\tau_i}{1+s\tau_i}\frac{\left[k^i - s\tau_o/(1+s\tau_o)\right]k_o^i k^o}{1 - [s\tau_i/(1+s\tau_i)][s\tau_o/(1+s\tau_o)]k_o^i k_i^o} A_z,$$
$$A_z^o = -\frac{s\tau_o}{1+s\tau_o}\frac{[k^o - s\tau_i/(1+s\tau_i)]k^i k_i^o}{1 - [s\tau_i/(1+s\tau_i)][s\tau_o/(1+s\tau_o)]k_o^i k_i^o} A_z. \tag{30}$$

The final expression, in canonical form, is

$$A_z^i = -s\tau_i \frac{k^i - s\tau_o\left(k_o^i k^o - k^i\right)}{1 + s(\tau_i + \tau_o) + s^2\left(1 - k_o^i k_i^o\right)} A_z,$$
$$A_z^o = -s\tau_o \frac{k^o - s\tau_i\left(k^i k_i^o - k^o\right)}{1 + s(\tau_i + \tau_o) + s^2\left(1 - k_o^i k_i^o\right)} A_z. \tag{31}$$

It is now possible to write the total potential vector $A_z^{tot}(r) = A_z(r) + A_z^i(r) + A_z^o(r)$ as a function of $A_z(r)$, produced by the source current, as follows:

$$A_z^{tot}(r) = A_z(r)\frac{1 + s\left[\tau_i\left(1 - k^i\right) + \tau_o(1 - k^o)\right] + s^2\tau_i\tau_o\gamma(r)}{1 + s(\tau_i + \tau_o) + s^2\tau_i\tau_o\left[1 - k_o^i k_i^o\right]}, \tag{32}$$

where $\gamma(r) = 1 - k^i - k^o + k^i k_i^o + k^o k_o^i - k_o^i k_i^o$.

As k^i, k^o, k_o^i, k_i^o all depend on r, the above expression is fully general and allows for the calculation of the total potential vector anywhere. From this general expression, it is easy to highlight the presence of a rational transfer function between $A_z(r)$ and $A_z^{tot}(r)$ that has two poles and two zeros. Only the position of the two zeros depends on r as

$$k_o^i(r)k_i^o(r) = \left(\frac{a}{c}\right)^{2n} = k_i k_o \le 1, \tag{33}$$

therefore, the coefficients of the denominator are fixed, hence the position of the poles. It is also straightforward to verify that such a transfer function is a minimum phase: the real part of both poles and zeros is negative (second-order polynomials with all positive coefficients; it can also be easily shown that the two poles are both real).

3. Circuital Model

3.1. Inductance. Equation (32) allows the calculation of the total magnetic potential vector everywhere; in particular, it allows to calculate it in the coils ($r = b$), and this is enough to calculate the inductance of the magnet (electrical terminals of the magnet are indeed located at $r = b$).

3.1.1. Potential Vector in the Coils. Note that

$$k^i(b) = k_i,$$
$$k^o(b) = k_o,$$
$$k_o^i(b) = k_i,$$
$$k_i^o(b) = k_o, \tag{34}$$

and introducing the following

$$k'_i = 1 - k_i,$$
$$k'_o = 1 - k_o, \tag{35}$$

the expression of the potential vector in the coils can be simplified as follows

$$A_z^{tot}(b) = A_z(b)\frac{1 + s\left(\tau_i k_i' + \tau_o k_o'\right) + s^2\tau_i\tau_o(1 - k_i - k_o + k_i k_o)}{1 + s(\tau_i + \tau_o) + s^2\tau_i\tau_o(1 - k_i k_o)}, \tag{36}$$

which can be rewritten to highlight its *dynamics* by means of the factor $\Lambda(s)$ as

$$A_z^{tot}(b, \theta, s) = A_z(b, \theta, s)\,\Lambda(s). \tag{37}$$

3.1.2. From Potential Vector to Inductance. In the quasistationary magnetic conditions assumed throughout this work, the stored magnetic energy can be calculated as

$$\mathcal{U} = \frac{1}{2}\iiint_V \mathbf{J}\cdot\mathbf{A}\,dv. \tag{38}$$

For the 2D approximation used herein, the stored energy per unit length is therefore

$$u = \frac{d\mathcal{U}}{dz} = \frac{1}{2}\iint_S \mathbf{J}\cdot\mathbf{A}\,ds, \tag{39}$$

where the surface S is the cross-section of the magnet; however, $\mathbf{J}$ is nonzero only for $r = b$.

Since the total potential vector at $r = b$ is simply the *source* potential vector times $\Lambda(s)$ (the transfer function in equation (37)), the energy per unit length can be easily calculated.

$$\begin{aligned} u &= \frac{1}{2}\iint_S J_z(r,\theta,s)\Lambda(s)A_z(r,\theta,s)r\,dr\,d\theta \\ &= \frac{1}{2}\Lambda(s)I^2(s)\frac{\mu_0 N_t^2}{8n}\frac{1}{b\Delta_b}b\Delta_b\int_0^{2\pi}\cos^2(n\theta)\,d\theta \\ &= \Lambda(s)\mu_0\frac{N_t^2 I^2(s)\pi}{16n}, \end{aligned} \tag{40}$$

where $\delta[(r-b)/\Delta_b]r\,dr$ has been integrated over all possible values of the radius whose result is equal to $b\Delta_b$.

The inductance per unit length ℓ can be derived from the energy per unit length as follows:

$$\ell = \frac{dL}{dz} = \frac{1}{I}\frac{\partial u}{\partial I}, \tag{41}$$

which gives

$$\ell = \Lambda(s)\mu_0\frac{N_t^2\pi}{8n} = \Lambda(s)\ell_{DC}. \tag{42}$$

The *static* or DC inductance can be written as

$$L_{DC} = \ell_{DC}l = \mu_0\frac{\pi N_t^2}{8n}l, \tag{43}$$

where l is the magnet length over the z axis (this expression coincides with the one reported in [4]).

Finally, the sought *dynamic inductance* can be expressed as

$$L(s) = L_{DC}\Lambda(s). \tag{44}$$

3.2. Equivalent Circuit. It can be verified that

$$\Lambda(s) = \frac{[1+s\tau_i(1-k_i)][1+s\tau_o(1-k_o)]}{1+s(\tau_i+\tau_o)+s^2\tau_i\tau_o(1-k_ik_o)}, \tag{45}$$

to which corresponds the equivalent circuit in Figure 2.

The proposed equivalent circuit represents a generalization of the one presented in [4]. It allows several considerations to be made:

(i) Not all the current supplied by the power converter $i_{circuit}$ is producing magnetic field in the *theoretical aperture* of the magnet ($r \le b$); indeed, a fraction i_o is shunted by the outer conductive layer

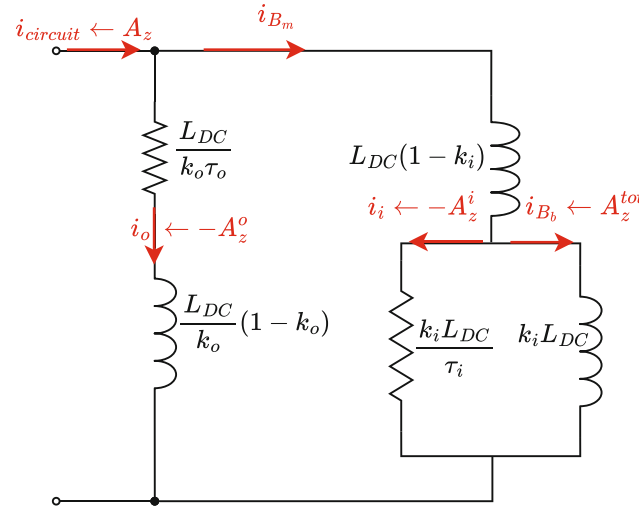

Figure 2: Full circuit model for a lossy superconducting magnet: inner and outer conducting shells.

(ii) The magnetic field within the magnet's aperture can be thought as produced by the current i_{B_m}

(iii) Not all of the field produced by i_{B_m} is actually seen by the beam in the interior of the inner conductive shell (such as the interior of a beam screen, $r \le a$)

(iv) There is indeed a shielding effect, and the difference between the field outside the inner layer ($a < r < b$) and the field inside the inner layer, ($r \le a$) can be thought as being produced by the difference current $i_i = i_{B_m} - i_{B_b}$

(v) In other terms, only the current i_{B_b} is producing the magnetic field seen by the beam

The equivalent circuit allows for an easy calculation of many interesting features. In particular, it allows studying the effect of power converter noise (both voltage and current) on the magnetic field seen by the beam inside the beam screen or vacuum pipe.

As an example, from equation (32), the TF (transfer function) between the vector potential in the region $r \le a$ with and without the inner and outer layers is the following:

$$\frac{A_z^{tot}(r\le a)}{A_z(r\le a)} = \frac{1+s\tau_o(1-k_o)}{1+s(\tau_i+\tau_o)+s^2\tau_i\tau_o(1-k_ik_o)}. \tag{46}$$

This TF can be deduced from the equivalent circuit, as in Figure 2, as

$$\frac{i_{B_b}}{i_{circuit}} = \frac{i_{B_b}}{i_{B_m}}\frac{i_{B_m}}{i_{circuit}} = \frac{1}{1+s\tau_i}\frac{(1+s\tau_i)[1+s\tau_o(1-k_o)]}{1+s(\tau_i+\tau_o)+s^2\tau_i\tau_o(1-k_ik_o)}. \tag{47}$$

The analogy between the equivalent circuit and the dynamics of the magnetic vector potential cannot be further generalized though as, for example, current i_o would be

flowing at $r = c$ whereas the proposed circuit is limited to the electrical terminals of the magnet, i.e., $r = b$. Nevertheless, the equivalent circuit represents still a very useful model, and indeed, one can derive many other figures of interest; as an example, the losses during the energy ramp up and ramp down phases can be calculated by the knowledge of i_i and i_o along with their respective *resistances* (easily derived by inspection of the equivalent circuit).

3.3. Noise Analysis. Equation (47) answers fully the question of how much noise passes from the $i_{circuit}$ to the magnetic field experienced by the beam ($r \le a$). The overall effect is an attenuation that at high frequency (higher than the frequencies of all poles and zeros) gets stronger by 20 per frequency decade. It is nevertheless clear from the equivalent circuit that the overall magnet impedance is smaller than that of a superconducting magnet that has no inner or outer layer because of the parallel branches (circuit admittance is larger). As such, for a given voltage noise contribution, the overall *circuit* current noise is larger for a magnet with inner/outer conductive layers with respect to an *ideal* one. Therefore, the relevant question is how a *real* magnet compares to an *ideal* one in terms of noise transfer from the power converter voltage to the magnetic induction field experienced by the beam.

The admittance of the circuit shown in Figure 3 is expressed by the following equation:

$$A_{circuit} = \frac{i_{circuit}}{v_{circuit}} = \frac{1}{R_c} \frac{1 + s(\tau_i + \tau_o) + s^2 \tau_i \tau_o (1 - k_i k_o)}{1 + s\,\tau_\Sigma + s^2 \left[\tau_c \left(\tau_i' + \tau_o'\right) + \tau_i \tau_o \gamma_{io}\right] + s^3 \tau_c \tau_i' \tau_o'}, \quad (48)$$

where

$$\begin{aligned} \tau_c &= \frac{L_{DC}}{R_c}, \\ \tau_\Sigma &= \tau_c + \tau_i + \tau_o, \\ \tau_i' &= (1 - k_i)\tau_i, \tau_o' = (1 - k_o)\tau_o, \\ \gamma_{io} &= 1 - k_i k_o. \end{aligned} \quad (49)$$

The TF of interest is the one from $v_{circuit}$ to i_{B_b} which is expressed in the following equation.

$$\begin{aligned} \frac{i_{B_b}}{v_{circuit}} &= \frac{i_{B_b}}{i_{circuit}} \frac{i_{circuit}}{v_{circuit}} \\ &= \frac{1}{R_c} \frac{1 + s\tau_o(1 - k_o)}{1 + s\,\tau_\Sigma + s^2 \left[\tau_c \left(\tau_i' + \tau_o'\right) + \tau_i \tau_o \gamma_{io}\right] + s^3 \tau_c \tau_i' \tau_o'}. \end{aligned} \quad (50)$$

Equation (50) shows that there are one zero and three poles, indicating a stronger attenuation of noise (in high frequency) w.r.t. the *no layers* case as expressed in the following equation

$$\left(\frac{i_{B_b}}{v_{circuit}}\right)^{no\ layers} = \frac{1}{R_c} \frac{1}{1 + s\tau_c}. \quad (51)$$

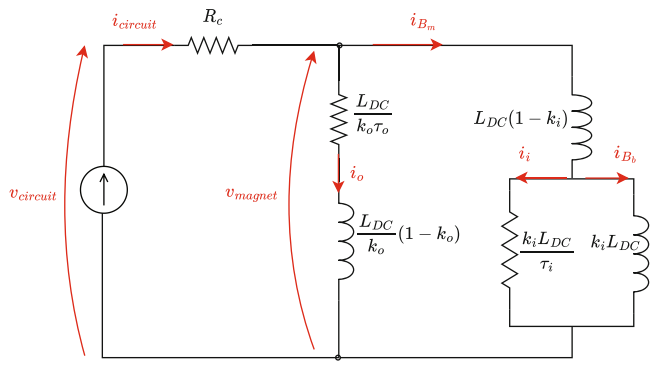

Figure 3: Full circuit model as seen from a power converter of a lossy superconducting magnet: inner and outer conducting shells. R_c represents the resistance of the normal conducting cables connecting the power converter to the superconducting magnet.

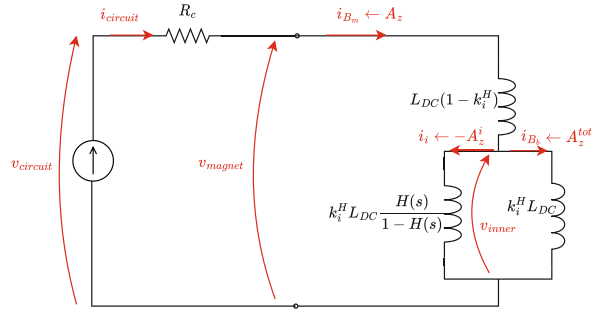

Figure 4: Circuit model seen from a power converter of a lossy superconducting magnet: most general inner conducting shell.

However, in such a form, i.e., equation (50), there is not much insight about the extra filtering; such expression can be considerably simplified noticing that $\tau_c >> \tau_i, \tau_o, \tau_i', \tau_o'$; hence, the following approximations hold:

$$\begin{aligned} \tau_\Sigma = \tau_c + \tau_i + \tau_o &\approx \tau_c + \tau_i' + \tau_\Sigma' = \tau_i', \\ \tau_c \left(\tau_i' + \tau_o'\right) + \tau_i \tau_o \gamma_{io} &\approx \tau_c \left(\tau_i' + \tau_o'\right) + \tau_i' \tau_o'. \end{aligned} \quad (52)$$

Combining equation (50) and the approximations in equation (52) gives

$$\begin{aligned} \frac{i_{B_b}}{v_{circuit}} &\approx \frac{1}{R_c} \frac{1 + s\tau_o(1 - k_o)}{1 + s\,\tau_\Sigma' + s^2 \left[\tau_c \left(\tau_i' + \tau_o'\right) + \tau_i' \tau_o'\right] + s^3 \tau_c \tau_i' \tau_o'} \\ &= \frac{1}{R_c} \frac{1 + s\tau_o'}{(1 + s\tau_c)\left(1 + s\tau_i'\right)\left(1 + s\tau_o'\right)} \\ &= \frac{1}{R_c} \frac{1}{(1 + s\tau_c)} \frac{1}{\left(1 + s\tau_i'\right)}. \end{aligned} \quad (53)$$

From equation (53), it is straightforward to deduce that

$$\frac{i_{B_b}}{v_{circuit}} \approx \left(\frac{i_{B_b}}{v_{circuit}}\right)^{no\ layers} \frac{1}{1+s\tau_i'} = \left(\frac{i_{B_b}}{v_{circuit}}\right)^{no\ layers} \frac{1}{1+s\tau_i(1-k_i)}. \tag{54}$$

Equation (54) shows that

(i) there is a first-order additional filtering effect

(ii) only the internal conductive layer (such as a beam screen) contributes to this additional filtering from voltage noise (to the magnetic field experienced by the beam) (in this respect, the usefulness of the proposed modelling holds even for practical magnets when the assumption of a *thin* layer for the stainless steel or Al collars does not)

(iii) the filtering occurs at higher frequencies compared to the filtering effect of the currents (or equivalently of the fields themselves)

(iv) the ratio i_{B_b}/i_{B_m} indeed depends on the time constant τ_i, whereas the ratio $i_{B_b}/(i_{B_b})^{no\ layers}$ depends on τ_i' and τ_i is larger than $\tau_i' = \tau_i(1-k_i)$ as $0 < k_i < 1$

4. General Model for Inner Layer

In the previous section, it was concluded that the dominant effect is the one due to the inner layer; in the Appendix, it will be shown that, considering only the inner layer, the proposed equivalent circuit is well defined even in the presence of an outer iron yoke. A generalization is now presented by means of the symbolic equivalent circuit shown in Figure 4. For such a circuit, where

$$H(s) = \frac{A_z^{tot}(s)}{A_z(s)}, \tag{55}$$

the TF of interest (i.e., between the power converter voltage and the current i_{B_b}) can be written as

$$\begin{aligned}\frac{i_{B_b}}{v_{circuit}} &= \frac{i_{B_b}}{v_{inner}} \cdot \frac{v_{inner}}{v_{magnet}} \cdot \frac{v_{magnet}}{v_{circuit}} \\ &= \frac{1}{sk_i^H L_{DC}} \cdot \frac{sk_i^H L_{DC} H(s)}{sL_{DC}\left[\left(1-k_i^H\right)+k_i^H H(s)\right]} \\ &\quad \cdot \frac{sL_{DC}\left[\left(1-k_i^H\right)+k_i^H H(s)\right]}{R_c + sL_{DC}\left[\left(1-k_i^H\right)+k_i^H H(s)\right]} \\ &= \frac{1}{R_c} \frac{H(s)}{1+s\tau_c\left[\left(1-k_i^H\right)+k_i^H H(s)\right]},\end{aligned} \tag{56}$$

where an equivalent geometrical factor k_i^H is replacing the one introduced in equation (7).

Equation (56) simplifies into equation (53) in the *thin* layer approximation whereby, from equation (9),

$$H(s) = \frac{A_z^{tot}(s)}{A_z(s)} = \frac{1}{1+s\tau_i}. \tag{57}$$

All conclusions drawn from equation (54) concerning the noise attenuation are hence valid irrespective to the validity of the *thin* layer approximation; in particular, the relevant fact that the additional noise attenuation (from voltage-to-current or voltage-to-field) becomes dominant at higher frequencies w.r.t. the current-to-current (or field-to-field) attenuation as $k_i^H \le 1$.

4.1. Full Analytical Formulation for a Dipole. For a dipole magnet, i.e., $n = 1$, an exact expression is available for the case of the inner conductive layer in the region $r < a$.

In [7], a general formula, equation (58), is reported where the thickness of the layer is not bounded to be much smaller than the radius a ; such a formula is also a generalization of the one presented in [8] (both of them only apply to dipole magnets, i.e., $n = 1$),

$$\frac{A_z^{tot}(r)}{A_z(r)} = \frac{2\mu_r[(a-\Delta/2)/(a+\Delta/2)]}{\left[\mu_r \mathrm{K}_1(\gamma_{a^-}) - \gamma_{a^-}\mathrm{K}_1'(\gamma_{a^-})\right]\left[\mu_r \mathrm{I}_1(\gamma_{a^+}) + \gamma_{a^+}\mathrm{I}_1'(\gamma_{a^+})\right] - \left[\mu_r \mathrm{I}_1(\gamma_{a^-}) - \gamma_{a^-}\mathrm{I}_1'(\gamma_{a^-})\right]\left[\mu_r \mathrm{K}_1(\gamma_{a^+}) + \gamma_{a^+}\mathrm{K}_1'(\gamma_{a^+})\right]}, \tag{58}$$

The quantities involved are as follows:

$$\begin{aligned}\gamma &\approx \sqrt{j2\pi f \mu_0 \mu_r \sigma^i} = \frac{1+j}{\delta}, \\ \gamma_{a^-} &= \gamma \cdot \left(a - \frac{\Delta}{2}\right), \\ \gamma_{a^+} &= \gamma \cdot \left(a + \frac{\Delta}{2}\right).\end{aligned} \tag{59}$$

where δ is the *penetration depth* of the conductive layer having an electrical conductivity σ^i. The functions involved are the first-order modified Bessel functions of first I_1 and second kind K_1 and their first derivatives (w.r.t. their argument). Assuming that $\mu_r = 1$ (which is an excellent approximation) and noting that

$$\begin{aligned}z\,K_1'(z) &= -zK_0(z) - K_1(z), \\ z\,I_1'(z) &= zI_0(z) - I_1(z),\end{aligned} \tag{60}$$

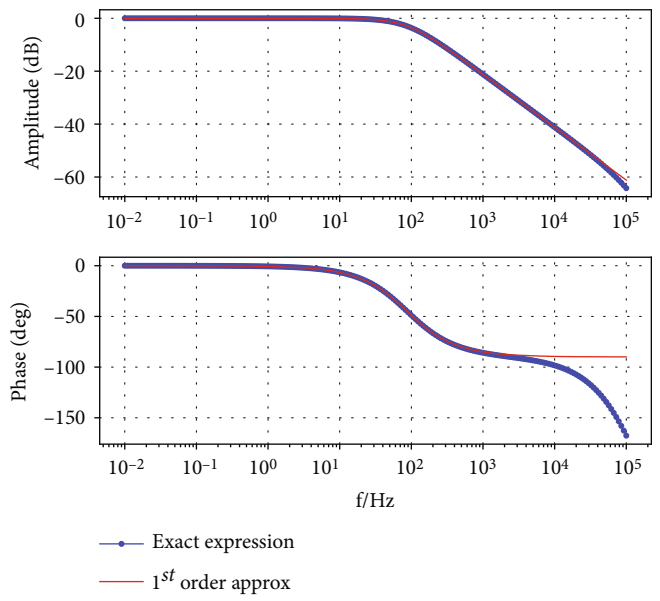

Figure 5: Bode plot comparison: equation (61) in blue vs. equation (57) in red. Top: amplitude; bottom: phase.

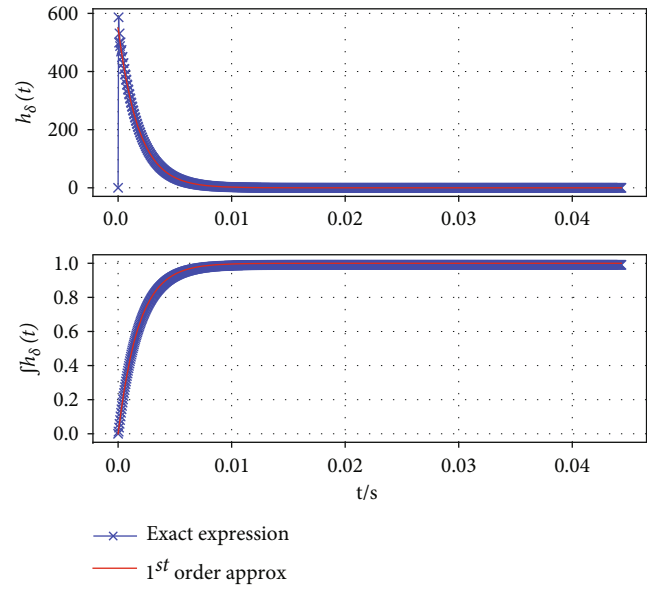

Figure 6: Impulse (top) and step (bottom) response comparison: equation (61) in blue vs. equation (57) in red.

Equation (58) can be considerably simplified to become equation (61),

$$\frac{A_z^{tot}(r)}{A_z(r)} = \frac{2[(a-\Delta/2)/(a+\Delta/2)]}{[2\,\mathrm{K}_1(\gamma_{a^-}) + \gamma_{a^-}\mathrm{K}_0(\gamma_{a^-})]\gamma_{a^+}\mathrm{I}_0(\gamma_{a^+}) + [2\,\mathrm{I}_1(\gamma_{a^-}) - \gamma_{a^-}\mathrm{I}_0(\gamma_{a^-})]\gamma_{a^+}\mathrm{K}_0(\gamma_{a^+})}. \tag{61}$$

4.1.1. Case of LHC Dipole. A numerical example is illustrated considering the case of the LHC dipoles. The cross-section of the LHC dipole beam screen is not perfectly circular; an equivalent first-order approximated TF is presented in [9]; however, such a cross-section can be assumed to be circular for comparison between the exact analytical model and the first-order one considered within the scope of this work. The whole beam screen is further approximated only with

the thin layer of copper, for which, however, the magnetoresistance effect (briefly discussed in the Appendix) is taken into account. The parameters used for the beam screen are the following: $a^- = (a - \Delta_a/2) = 18.45\,\text{mm}$, $\Delta_a = 75\,\mu\text{m}$, and $\sigma^i = 2.09 \times 10^9 \text{Sm}^{-1}$ (at 20 K and 8 T). The comparison between the exact expression in equation (61) and the first-order approximation, equation (57), is illustrated in Figure 5 in the frequency domain and Figure 6 in the time domain. It can be observed that the impulse response (impulse response $h_\delta(t) = \mathcal{F}^{-1}[H(s = j2\pi f)]$) of the *exact* TF is zero at $t = 0$ (Figure 6, top) which is a consequence of the fact that the TF is of an order larger than 1; indeed, its phase response (Figure 5, bottom) goes beyond the asymptote of -90° of the 1st order, thin layer, approximation. The overall agreement is excellent up to about 10 kHz whereas, looking only at the amplitude (which is the relevant one for noise considerations), a very good agreement is maintained even beyond about 20 kHz when the penetration depth δ becomes equal to the shell thickness; this is an important result which confirms the validity of the *thin* layer approximation presented and its relevance for existing and next-to-come particle accelerators.

5. Conclusion

A quasistationary magnetic model of an ideal superconducting magnet has been presented. Although idealized, the model includes all the important constituents of practical particle accelerators magnets: the beam screen, the iron yoke (addressed in the Appendix), and the collar. The model has been translated into an equivalent circuit generalizing the one presented in [4]. Such an equivalent circuit has been exploited to carry out a noise analysis focusing on the final impact of power converter voltage noise on the magnetic field to be experienced by the beam. A quantitative, although approximated, estimation of additional noise attenuation (w.r.t. a pure inductance model of the magnet) has also been presented and represents the main result of this work. Non-*thin* inner and outer layers have been briefly addressed in this context, whereas the coils' layer is discussed with more details in the Appendix where the validity of the presented model is shown to hold.

Appendix

A. Iron Yoke

The presence of a *thick* concentric iron yoke, with relative permeability μ_r and inner radius d (outer radius is assumed large enough not to be considered), as shown in Figure 7 can be accounted for, following [5], by means of the equivalence with an *image* current I' located at radius b' such that

$$b' = \frac{d^2}{b}, \tag{A.1}$$

$$I' = \frac{\mu_r - 1}{\mu_r + 1} I. \tag{A.2}$$

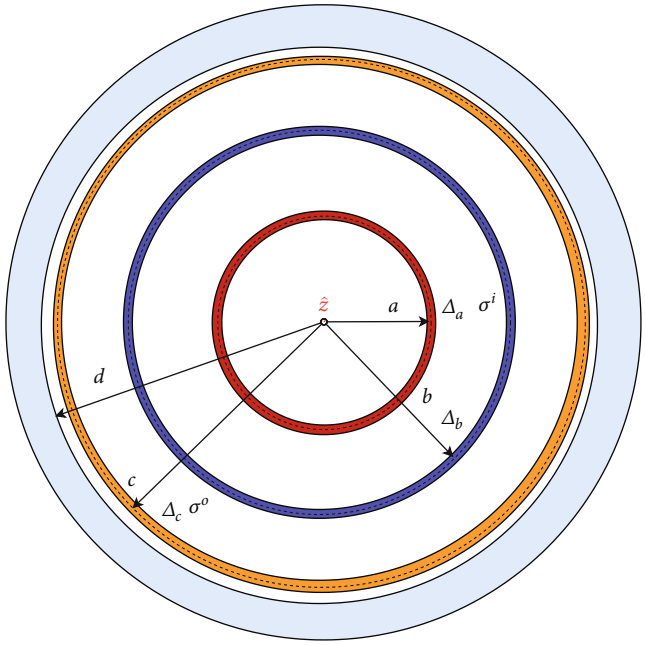

Figure 7: Simplified cross-section (not to scale) of an ideal superconducting magnet with an iron yoke with inner radius d.

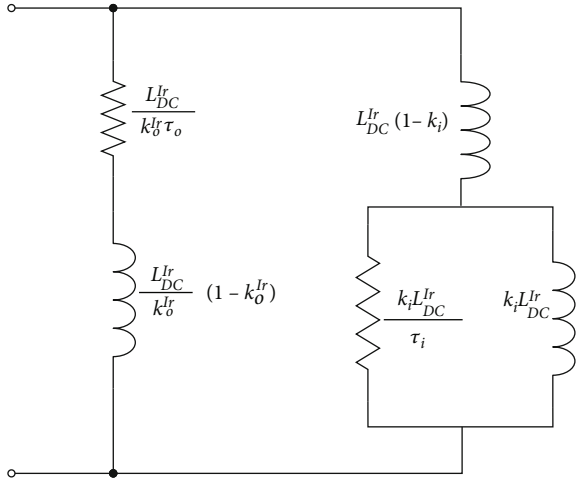

Figure 8: Approximate circuit model for a lossy superconducting magnet: inner and outer conducting shells with an iron yoke.

This equivalence is valid for $r \le d$; the resulting potential vector $A_z^t(r)$ would be

$$A_z^t(r) = \mu_0 \frac{b\Delta_b}{2n} \left(\frac{r}{b}\right)^{n\ \text{sgn}\,(b-r)} J_z(b) + \mu_0 \frac{b'\Delta_{b'}}{2n} \left(\frac{r}{b'}\right)^{n\ \text{sgn}\,(b'-r)} J_z'(b'). \tag{A.3}$$

Following again [5], it can be observed that

$$J_z'(b')\Delta_{b'} = \frac{\mu_r - 1}{\mu_r + 1} \left(\frac{b}{d}\right)^2 J(b)\Delta_b. \tag{A.4}$$

From equations (A.1), (A.2), and (A.4), it is easy to see that

$$J_z'\left(b'\right)b'\Delta_{b'} = \frac{\mu_r - 1}{\mu_r + 1} J(b) b \Delta_b. \tag{A.5}$$

So, equation (A.3) can be finally rewritten as

$$A_z^t(r) = \mu_0 \frac{b\Delta_b}{2n} \left(\frac{r}{b}\right)^{n\ \mathrm{sgn}\,(b-r)} J_z(b) \left[1 + \frac{\mu_r - 1}{\mu_r + 1} \left(\frac{r}{b}\right)^{n\ \mathrm{sgn}\,(r-b)} \left(\frac{r}{b'}\right)^{n\ \mathrm{sgn}\,\left(b'-r\right)}\right]. \tag{A.6}$$

In the region $r \le d$, equation (A.6) can be further simplified in

$$A_z^t(r) = A_z(r)[1 + \beta(r)], \tag{A.7}$$

where

$$\beta(r) = \frac{\mu_r - 1}{\mu_r + 1} \left(\frac{b}{d}\right)^{2n} \left(\frac{r}{b}\right)^{n[1-\mathrm{sgn}\,(b-r)]}. \tag{A.8}$$

The mathematical derivation of the general case of both inner and outer conductive layers without iron yoke has been carried out in Section 2, in particular, equations (18) and (19) for the inner layer and equations (21) and (22) for the outer.

Analogously to what is done in equation (18), the contribution to the inner layer with the iron yoke present can be written as

$$\begin{aligned} A_z^i(r) &= \mu_0 \frac{a\Delta_a}{2n} \left(\frac{r}{a}\right)^{n\ \mathrm{sgn}\,(a-r)} J_z^i(a) = \mu_0 \frac{a\Delta_a}{2n} \left(\frac{r}{a}\right)^{n\ \mathrm{sgn}\,(a-r)} \left[-s\sigma^i A_z^{tot}(a)\right] \\ &= -s\tau_i \left(\frac{r}{a}\right)^{n\ \mathrm{sgn}\,(a-r)} \left[A_z^t(a) + A_z^i(a) + A_z^o(a)\right] \\ &= -s\tau_i \left(\frac{r}{a}\right)^{n\ \mathrm{sgn}\,(a-r)} \left\{[1 + \beta(a)]A_z(a) + A_z^i(a) + A_z^o(a)\right\}. \end{aligned} \tag{A.9}$$

Analogously to what is done in equation (19), equation (A.9) can be factorized as

$$A_z^i(r) = -s\tau_i \left[k_{Ir}^i(r) A_z(r) + A_z^i(r) + k_o^i(r) A_z^o(r)\right], \tag{A.10}$$

where a new positional function is introduced:

$$k_{Ir}^i(r) = k^i(r) \frac{1 + \beta(a)}{1 + \beta(r)}. \tag{A.11}$$

For the outer layer, equation (21) would now read as

$$\begin{aligned} A_z^o(r) &= \mu_0 \frac{c\Delta_c}{2n} \left(\frac{r}{c}\right)^{n\ \mathrm{sgn}\,(c-r)} J_z^o(c) = \mu_0 \frac{c\Delta_c}{2n} \left(\frac{r}{c}\right)^{n\ \mathrm{sgn}\,(c-r)} \left[-s\sigma^o A_z^{tot}(c)\right] \\ &= -s\tau_o \left(\frac{r}{c}\right)^{n\ \mathrm{sgn}\,(c-r)} \left[A_z^t(c) + A_z^i(c) + A_z^o(c)\right] \\ &= -s\tau_o \left(\frac{r}{c}\right)^{n\ \mathrm{sgn}\,(c-r)} \left\{[1 + \beta(c)]A_z(c) + A_z^i(c) + A_z^o(c)\right\}, \end{aligned} \tag{A.12}$$

whereas equation (22) would read as

$$A_z^o(r) = -s\tau_o \left[k_{Ir}^o(r) A_z(r) + k_i^o(r) A_z^i(r) + A_z^o(r)\right], \tag{A.13}$$

where

$$k_{Ir}^o(r) = k^o(r) \frac{1 + \beta(c)}{1 + \beta(r)}. \tag{A.14}$$

By means of the k_{Ir}^i and k_{Ir}^o functions, the total magnetic potential including the effect of the iron core can be written in a form completely analogous to equation (32):

$$A_z^{tot} = A_z[1 + \beta(r)] \frac{1 + s\left[\tau_i\left(1 - k_{Ir}^i\right)\right] + \tau_o(1 - k_{Ir}^o)] + s^2\tau_i\tau_o\gamma_{Ir}(r)}{1 + s(\tau_i + \tau_o) + s^2\tau_i\tau_o\left(1 - k_o^i k_i^o\right)}, \tag{A.15}$$

where $\gamma_{Ir}(r) = 1 - k_{Ir}^i - k_{Ir}^o + k_{Ir}^i k_i^o + k_{Ir}^o k_o^i - k_o^i k_i^o$.

All the considerations made about the position of the zeros and the poles remain valid in the presence of an iron yoke. In particular, in order to determine what is *seen* at the circuit terminals, i.e., $r = b$, the following constants are needed:

$$\begin{aligned} k_{Ir}^i(b) &= k^i(b) \frac{1 + \beta(a)}{1 + \beta(b)} = k^i(b) = k_i, \\ k_{Ir}^o(b) &= k^o(b) \frac{1 + \beta(c)}{1 + \beta(b)} = k_o \frac{1 + \beta(c)}{1 + \beta(b)} = k_o^{Ir}, \\ \gamma_{Ir}(b) &= 1 - k_i - k_o^{Ir} + k_i k_o + k_o^{Ir} k_i - k_i k_o = (1 - k_i)\left(1 - k_o^{Ir}\right). \end{aligned} \tag{A.16}$$

B. Inductance and Approximated Equivalent Circuit

For what the inductance is concerned about, its DC value depends only on the total vector potential at $r = b$; it is therefore pretty straightforward to deduce that

$$L_{DC}^{Ir} = L_{DC}[1 + \beta(b)] = L_{DC} \left[1 + \frac{\mu_r - 1}{\mu_r + 1} \left(\frac{b}{d}\right)^{2n}\right]. \tag{B.1}$$

As for equation (44), the *dynamic inductance* can be written as

$$L_{Ir}(s) = L_{DC}^{Ir} \Lambda_{Ir}(s), \tag{B.2}$$

where

$$\Lambda_{Ir}(s) = \frac{1 + s\left[\tau_i(1-k_i) + \tau_o\left(1-k_o^{Ir}\right)\right] + s^2\tau_i\tau_o\gamma_{Ir}(b)}{1 + s(\tau_i+\tau_o) + s^2\tau_i\tau_o(1-k_ik_o)} = \frac{\left[1+s\tau_i(1-k_i)\right]\left[1+s\tau_o\left(1-k_o^{Ir}\right)\right]}{1 + s(\tau_i+\tau_o) + s^2\tau_i\tau_o(1-k_ik_o)}. \tag{B.3}$$

Unfortunately, there is no equivalent circuit to equation (B.3) as it exists for equation (45).

However, an approximate equivalent circuit as the one depicted in Figure 8 can still be devised; its impedance would be

$$Z_{Ir}(s) = \frac{\left[1+s\tau_i(1-k_i)\right]\left[1+s\tau_o\left(1-k_o^{Ir}\right)\right]}{1 + s(\tau_i+\tau_o) + s^2\tau_i\tau_o\left(1-k_ik_o^{Ir}\right)}. \tag{B.4}$$

The position of the zeros of the *equivalent circuit* is identical, whereas the position of the poles is slightly off. It should also be noted that for reasonable magnet geometries, the factor k_{Ir}^o would not be significantly different from k^o, so finally the equivalent circuit is still a rather accurate approximation. Furthermore, since the factors k_{Ir}^i and k^i are exactly the same and that the inner layer is the dominant one for the noise analysis (as already shown), it can be safely stated that the presence of the iron yoke does not affect at all the conclusions drawn so far. It is important to note that even if the presented *dynamic inductance* could have a more general validity by assuming $\mu_r = \mu_r(I,s)$ (i.e., μ_r being a function of both the current intensity I and its frequency), it should be considered hereby as a valid model only for small current variations around a given steady current level; as such, it is perfectly suited for noise analysis purposes.

C. Finite Coil Thickness

In the case of finite thickness of the coils, i.e., when Δ_b is not negligibly small compared to b, the quasistatic current density is assumed to be constant between the inner and outer radii $b^{\pm} = b \pm \Delta_b/2$ and zero elsewhere ($\Pi[(r-b)/\Delta_b] = u[r-(b-\Delta_b/2)] - u[r-(b+\Delta_b/2)]$ where $u(.)$ is the Heaviside function):

$$J_z(r,\theta,s) = \frac{N_t\cos(n\theta)}{2} I(s)\frac{1}{b\Delta_b}\Pi\left(\frac{r-b}{\Delta_b}\right). \tag{C.1}$$

The magnetic vector potential produced by this new current density can be calculated as follows [6]:

$$A_z(r,\theta,s) = \frac{\mu_0}{2n}\frac{N_tI(s)}{2}\cos(n\theta)\frac{1}{b\Delta_b} \cdot \begin{cases} r^n\displaystyle\int_{b^-}^{b^+}\lambda^{1-n}\mathrm{d}\lambda, & r < b^-, \\ r^n\displaystyle\int_{b^-}^{r}\lambda^{1-n}\mathrm{d}\lambda + r^{-n}\int_{r}^{b^+}\lambda^{1+n}\mathrm{d}\lambda, & b^- < r < b^+, \\ r^{-n}\displaystyle\int_{b^-}^{b^+}\lambda^{1+n}\mathrm{d}\lambda, & r > b^+, \end{cases} \tag{C.2}$$

where the integration variable λ spans the radius of the coils. In this case, the different transfer functions that have been calculated so far would need to be modified accordingly. However, by means of Taylor expansion in terms of the relative thickness Δ_b/b, it can be shown that

$$A_z(r,\theta,s) = \frac{\mu_0}{2n}\frac{N_tI(s)}{2}\cos(n\theta) \cdot \begin{cases} \left(\dfrac{r}{b}\right)^n\left[1 + \dfrac{n(n-1)}{24}\left(\dfrac{\Delta_b}{b}\right)^2 + \cdots\right], & r < b^-, \\ \left(\dfrac{b}{r}\right)^n\left[1 + \dfrac{n(n+1)}{24}\left(\dfrac{\Delta_b}{b}\right)^2 + \cdots\right], & r > b^+, \end{cases} \tag{C.3}$$

where only powers greater or equal to 2 appear. Neglecting those terms will result in an expression identical to the (ideal) one in equation (1). Calculating now the vector potential in the coil region ($b^- < r < b^+$) and then the energy and again expanding in Taylor series, it can be shown that the inductance has the following expression:

$$L_{DC} = \mu_0\frac{\pi N_t^2}{8n}l\left[1 + \frac{n}{3}\left(\frac{\Delta_b}{b}\right) + \frac{n^2}{12}\left(\frac{\Delta_b}{b}\right)^2 + \cdots\right], \tag{C.4}$$

where the dominant contribution is given by the first power of the relative thickness. Therefore, the proposed analytical model, derived with the assumption of (infinitely) thin coils layer, still holds when it is possible to neglect powers greater than 1 of the relative thickness of the coils by simply correcting the inductance with the factor: $1 + (n/3)(\Delta_b/b)$.

D. Magnetoresistance

The electrical conductivity of copper and other metals is affected by the intensity of the magnetic field they are exposed to, and such intensity depends finally on the circuit current. As such, the electrical conductivities considered so far are σ^i and σ^o, and therefore, also the time constants τ_i and τ_o would depend on the intensity of the circuit current,

so the equivalent circuit proposed in the Circuital Model would be slightly nonlinear.

However, as for the effect of the iron yoke, the noise analysis could still be carried out accurately for any operational *steady* current level (flat-top, injection, etc.).

Data Availability

This work is essentially an analytical modelling one, so it does not rely on data supporting its results.

Conflicts of Interest

The author declares that they have no conflicts of interest.

Acknowledgments

Research is supported by the HL-LHC project. The author would like to thank Antonio Esposito for his contribution on the field modelling.

References

[1] I. Béjar Alonso, O. Brüning, P. Fessia, L. Rossi, L. Tavian, and M. Zerlauth, *High-Luminosity Large Hadron Collider (HL-LHC): Technical Design Report*, CERN Yellow Reports: Monographs, CERN, Geneva, 2020.

[2] D. Gamba, G. Arduini, M. Cerqueira Bastos et al., *Beam dynamics requirements for HL–LHC electrical circuits*, CERN, Geneva, 2017.

[3] D. Gamba, R. Tomas Garcia, M. Giovannozzi et al., *Update of beam dynamics requirements for HL-LHC electrical circuits*, CERN, Geneva, 2019.

[4] R. Shafer, "Eddy currents, dispersion relations, and transient effects in superconducting magnets," *IEEE Transactions on Magnetics*, vol. 17, no. 1, pp. 722–725, 1980.

[5] P. Schmuser, "Superconducting magnets for particle accelerators," *Reports on Progress in Physics*, vol. 54, no. 5, pp. 683–730, 1991.

[6] R. Gupta, *Field calculations and computations*, School at CAT, Indore, India, 1998.

[7] S. Celozzi, R. Araneo, and G. Lovat, *Electromagnetic shielding*, John Wiley & Sons, 2008.

[8] F. Zimmermann, *Emittance growth and proton beam lifetime in HERA, [Ph.D. thesis]*, Hamburg U, 1993.

[9] M. Morrone, M. Martino, R. De Maria, M. Fitterer, and C. Garion, "Magnetic frequency response of High-Luminosity Large Hadron Collider beam screens," *Physical Review Accelerators and Beams*, vol. 22, article 013501, 2019.